Functional Composite Materials

RESEARCH

Open Access

Heat treated graphene thin films for reduced void content of interlaminar enhanced CF/PEEK composites

Christopher Leow[1*], Peter B. Kreider[1], Silvano Sommacal[1], Christian Notthoff[2], Patrick Kluth[2] and Paul Compston[1,2]

Abstract

Graphene enhanced thermoplastic composites offer the possibility of conductive aerospace structures suitable for applications from electrostatic dissipation, to lightning strike protection and heat dissipation. Spray deposition of liquid phase exfoliated (LPE) aqueous graphene suspensions are highly scalable rapid manufacturing methods suitable to automated manufacturing processes. The effects of residual surfactant and water from LPE on thin films for interlaminar prepreg composite enhancement remain unknown. This work investigates the effect of heat treatment on graphene thin films spray deposited onto carbon fibre/polyether ether ketone (CF/PEEK) composites for reduced void content. Graphene thin films deposited onto CF/PEEK prepreg tapes had an RMS roughness of 1.99 µm and an average contact angle of 11°. After heat treatment the roughness increased to 2.52 µm with an average contact angle of 82°. The SEM images, contact angle, and surface roughness measurements correlated suggesting successful removal of excess surfactant and moisture with heat treatment. Raman spectroscopy was used to characterise the chemical quality of the consolidated graphene interlayer. Spectral data concluded the graphene was 3–4 layered with predominantly edge defects suggesting high quality graphene suitable for electrical enhancement. Conductive-AFM measurements observed an increase in conductive network density in the interlaminar region after the removal of surfactant from the thin film. Heat treatment of the Control sample successfully reduced void content from 4.2 vol% to 0.4 vol%, resulting in a 149% increase in compressive shear strength. Comparatively, heat treatment of graphene enhanced samples (~ 1 wt%) reduced void content from 5.1 vol% to 2.8 vol%. Although a 25% reduction in shear strength was measured, the improved electrical conductivity of the interlaminar region extends the potential applications of fibre reinforced thermoplastic composites. The heat treatment process proves effective in reducing surfactant and thus void content while improving electrical conductivity of the interlayer in a scalable manner. Further investigations into graphene loading effects on conductive enhancement, and void formation is needed.

Keywords Nanocomposite, Nanomaterials, Thermoplastics, Graphene, Thin films

Introduction

Cross-linked thermosetting carbon fibre reinforced polymers (CFRP) are difficult to recycle, and thermoplastics are a suitable alternative due to their recyclability and repairability capabilities necessary for long service life CFRP aerospace vehicles. Polyether ether ketone (PEEK) is a high performance thermoplastic with high melting temperature, strength and chemically resistant properties

*Correspondence:
Christopher Leow
christopher.leow@anu.edu.au
[1] ARC Training Centre for Automated Manufacture of Advanced Composites, Australian National University, Canberra, ACT 2601, Australia
[2] Research School of Physics, College of Science, Australian National University, Canberra, ACT 2601, Australia

that make it highly suitable for operation in aerospace environments [1, 2].

The intrinsic conductivity properties of PEEK make it unsuitable for electrostatic discharge, or thermal dissipation applications without an additional enhancing material [3]. Graphene has high specific area, tensile strength and thermal and electrical properties [4, 5] making it an excellent material to add electromagnetic interference [6], lightning strike [7] and electrostatic dissipation [8] functions to CFRP.

To ensure excellent graphene properties careful selection of synthesis methods are required. Chemical vapour deposition (CVD) methods and template growth offer high quality graphene at low scalability [9], while mechanical exfoliation and graphene oxide methods are limited in their purity, and toxic chemical by products [10, 11]. Liquid phase exfoliation (LPE) offers a scalable method to manufacture high quality and purity graphene in large volumes at low cost [9, 12].

High concentration graphene exfoliated in aqueous solutions offer economic and environmental advantages over solvent based suspensions [10, 13]. Surfactants aid exfoliation of nanomaterials while also ensuring dispersion in the liquid phase and reducing agglomeration effects over time [14]. Various surfactants have been used in aqueous suspensions [15-17], but tri-block copolymers have demonstrated the ability to synthesise high quality and highly stable suspensions without the need of centrifugation, promoting industrial relevance [18].

Spray deposition is compatible with LPE production methods and offers a scalable process to deposit nanomaterials onto composite substrates. Enhancement of the interlayer regions enables a method to develop nanomaterial enhanced CFRP with tailorable properties that is non-disruptive to composite manufacturing [19]. Li et al. [20] spray deposited a carbon nanotube (CNT)/graphene nanoplatelet (GNP) mixture onto aerospace grade CF/epoxy prepreg tapes for enhanced thermal and electrical conductivity. Zhang et al. [21] spray deposited CNTs suspended in methanol onto CF/epoxy prepreg tapes for improved fracture toughness properties. Thick interleaved graphene film (25–140 μm) additions to CF/epoxy composites have resulted in significant thermal and electrical conductivity increases at the detriment of interlaminar bonding due to hindered resin flow [22]. Thinner MWCNT interleaf additions (0.15 μm) manufactured using CVD methods resulted in reduced interlaminar strength properties due to localised resin evaporation, yet demonstrated successful lightning strike protection (74 Scm^{-1}) [23].

This study expands on earlier work aiming to reduce the voids previously observed within interlaminar graphene enhanced composites [24]. This work focuses on the heat treatment of graphene thin films on CF/PEEK prepreg tapes as a suitable method to reduce voids in consolidated composites. High concentration aqueous graphene suspensions were made with Pluronic triblock copolymer F68 as the surfactant using LPE methods and aerosolised to generate thin films. The thin films were characterised before and after heat treatment for uniformity, roughness, nanostructural characteristics, graphene quality, and wettability using optical microscopy, white light interferometry (WLI), scanning electron microscopy (SEM), Raman and FTIR spectroscopy, and a goniometer, respectively. The graphene enhanced CF/PEEK tapes were then consolidated in a hot press and the interlaminar regions studied using Raman spectroscopy, and SEM. Interlaminar shear strength and conductive networks were studied using compression shear testing and conductive atomic force microscopy (C-AFM), respectively. Micro-computed tomography (μCT) provided microstructural, void content and distribution information in three dimensions.

Materials and methods

Materials

Concentrated aqueous graphene suspensions (1.5 wt%) were synthesized through LPE methods [15]. Graphite (~1 μm flake size) starting material was exfoliated in a high-volume ultrasonic flow cell with continuous addition of non-ionic pluronic F68 surfactant (Sigma Aldrich). The AS-4 CF/PEEK (40 mm × 90 mm) unidirectional tapes (Toray Cetex, fibre volume fraction 59%) were used as the substrates to study the graphene thin film.

Spray deposition

The methodology applied to fabricate graphene interlayer enhanced CF/PEEK composites using spray deposition methodologies follows the same approach reported in an earlier work Leow et al. [24] (Fig. 1a). Average graphene flake size in the spray deposited thin films was measured to be 1.59 ± 0.47 μm. The aqueous graphene suspension was aerosolised at 1 bar air pressure fed through a NE-300 syringe pump (New Era Pump Systems Inc.) at a feed rate of 5 $mLmin^{-1}$. Deposition was done using a flat fan air atomising nozzle (SUE15, Xinhou Industrial Co. Ltd) onto CF/PEEK ply substrates from a distance of 300 mm for 30 s followed by drying on a hot plate at 50 °C for five minutes; this deposition process was defined as a pass and repeated to generate graphene thin films of varying thickness. The CF/PEEK plies were sprayed with ten passes (32 ± 1.5 mg) of F68 stabilised graphene suspension to create thin films that were further dried at room temperature for a minimum of 24 h. The nineteen graphene enhanced CF/PEEK plies were heat treated in

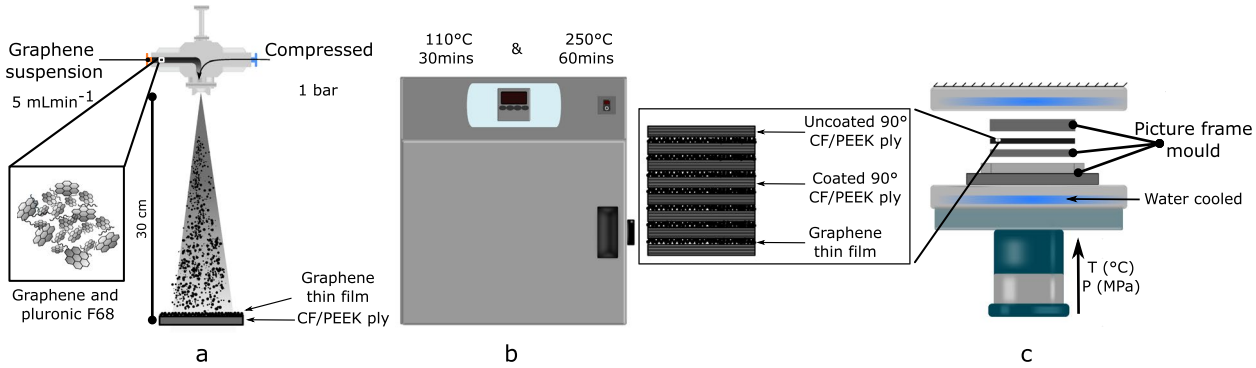

Fig. 1 **a** Aerosolised spray-deposition of the graphene suspension (graphically depicted in the inset) onto CF/PEEK ply substrate. **b** Scientific oven used for heat treatment of thin films and CF/PEEK plies. **c** Schematic of water-cooled hot press and picture frame mould used to manufacture consolidated composites. Partial unidirectional layup with graphene interlayers is illustrated in the inset

an oven (O75, Steridium) at 110 °C for 30 min to remove any water absorbed (Fig. 1b). The temperature was then raised to 250 °C for 60 min to vapourise excess non-ionic pluronic surfactant, following the methodology outlined in the Supporting Information of Mansukhani et al. [25], and were then cooled at a rate of ~ 20 °C/min.

Hot press consolidation

Consolidated composites were manufactured using a hot press (PW220C-X4A, Phi Hydraulics) in a picture frame mould following the methodology outlined in Cogswell [26] (Fig. 1c). The mould was heated in the hot press at 385 °C for 20 min under contact pressure conditions, then 1 MPa consolidation pressure was applied for 20 min (1 min/ply). The mould was water cooled with pressure maintained at a rate of ~ 40 °C/min until temperature dropped below T_g (140 °C). A single set of nineteen graphene enhanced CF/PEEK plies were laid up unidirectionally with an unmodified ply on top to create a $[(90)_{20}]$ composite layup with ~ 1 wt% graphene thin film interlayer additions. The consolidated CF/PEEK laminate without graphene additions will henceforth be referred to as Control, and with heat treatment Control (HT). Consolidated composite laminates with ~ 1 wt% graphene loadings will be referred to as GL and with additional heat treatment GL (HT). In total four laminated composites were synthesized in this study. Graphene thin film samples will be referred to as GTF and with heat treatment GTF (HT).

Sample preparation

The consolidated CF/PEEK samples were cut into 10 mm × 10 mm coupons using a waterjet cutter (Protomax, OMAX) and immediately ready for compressive shear testing. Subsequently they were also cast in epoxy resin to allow for the creation of material samples that enable direct measurement of interlaminar spaces by viewing the composites in cross-section. Three 10 mm × 10 mm coupons were secured end-on flush against the base of the resin-casting mould using double sided tape. The samples were then cast in epoxy resin (EpoFix) and de-gassed under vacuum for ~ 1 min to remove bubbles prior to a 24-h cure.

The resin cast coupons were then sliced into 1.5 mm thick disks using a gravity pressure fed diamond metal bonded wafering blade (Allied High Tech Productions Inc.). The samples were then mounted onto metallic holders with double sided tape and polished on an Allied MetPrep3 (Allied High Tech Productions Inc.) using polishing pads with the corresponding polishing suspensions. The samples were pre-polished in a clockwise rotating platen (200 rpm) and a clockwise sample head (150 rpm) with 17 N applied force for one minute with P-400, P-1200 and P-2400 on SiC polishing paper (FEPA grit sizes). They were then sequentially polished for four minutes with green lube and 6 µm and then 3 µm polycrystalline diamond glycol-based suspension on gold label woven nylon polishing pads (Allied High Tech Productions Inc.). Final polishing was conducted for four minutes on white label woven low-nap silk and polished using a mix of green lube and 1 µm polycrystalline diamond glycol-based suspension (Allied High Tech Productions Inc.). Polished samples were cleaned and dried with soap and compressed air respectively between changes in grits. The final polished epoxy embedded composite disks were used for interlaminar investigations using Raman spectroscopy and SEM.

The C-AFM polished resin embedded cross sectional samples were additionally painted with conductive silver paste and a Ø13mm metallic disk attached to create a conductive and physical contact. The coupons were further reduced in size for µCT imaging. They were cut

on a VC50 gravity pressure fed cutting machine using a 127 mm × 0.36 mm (diameter x thickness) diamond blade at 4 m/min (Leco, USA). Final sample dimensions for μCT were 10 mm × 2.5 mm × 3 mm (length x width x thickness).

Characterisation

The LPE synthesised graphene suspension was diluted and characterised using a UV–Vis spectrophotometer (Cary 60, Agilent) to attain absorbance (A) measurements from 200 to 1100 nm. The concentration (C) was calculated according to the Lambert–Beer law (Eq. 1) [16] using an extinction coefficient (α) of 5422 $mgmL^{-1}$ m^{-1} [27]. The resultant calculated concentration was 0.003 $mgmL.^{-1}$; which is more concentrated than previously studied [24]

$$A = \alpha LC \tag{1}$$

Optical microscopy, WLI and SEM

Qualitative validation of the spray-deposited graphene thin film was conducted on both macro and micro scales performed by using an optical microscope (Eclipse E200, Nikon) with a DS-Vi1 camera (Nikon) and electron microscope (FE-SEM UltraPlus, Zeiss). The graphene thin films were carbon coated to reduce charging effects from the PEEK substrate during electron imaging. Quantitative analysis of thin film surface topography and roughness was conducted on VEECO Wyko NT9100 Optical Profiling System using Vertical Scanning Interferometry (VSI) at a magnification of × 5. Five scans were taken at different locations on the samples to gain an average absolute and root-mean-square (RMS) roughness measurement.

FT-IR spectroscopy and contact angle measurements

Fourier transform infrared (FTIR) spectroscopy was conducted on the graphene thin films and CF/PEEK substrates, before and after heat treatment, to assess the moisture content and any chemical changes. The spectra was acquired on an FTIR spectrometer with a platinum ATR crystal (Alpha II, Bruker) from 4000–400 cm^{-1} and the data analysed in Origin 2018. Contact angle measurements were conducted with water on the graphene thin film with and without heat treatment. A 1 μL droplet of water was dispensed and imaged on a contact angle analyser (Phoenix MT Touch, Surface Electro Optics) with a 3° camera tilt relative to the sample stage.

Raman spectroscopy

The graphene quality of the generated thin films was chemically characterised on a confocal Raman microscope (Renishaw inVia Reflex) at a magnification of × 100. Samples were exposed to a 532 nm wavelength laser at 0.5 mW power with use of a 2400 mm^{-1} grating to isolate the signal and measurements were integrated over a period of 10 s with 3 accumulations to reduce signal to noise ratios. The spectral data was baseline corrected and normalised against the G peak using Spectragryph [28] and peak fitted using Origin 2018.

Conductive-atomic force microscopy (C-AFM)

The interlayer regions of graphene enhanced CF/PEEK composites were mapped with C-AFM (Dimension icon, Bruker) with conductive Platinum-Iridium tips. Measurements were conducted at ambient conditions using SCM-PIC-V2 (Bruker) probes set to a spring constant of 0.1 N/m. Current mapping of an area of 20 μm^2 was conducted in contact mode with a 0.5 V deflection set point maintained with a sample bias of 100 mV. Mean grey average optical density measurements of the C-AFM maps were conducted in ImageJ (calibrated with a Kodak No. 3 step tablet [29]). The pixel colours ranged from back (0) to white (255) and were indexed to the lowest (black) to highest (white) current measurements, respectively.

Compression shear testing

The compression shear testing device and technique follows the methodology outlined for flat specimens in Zinnecker et al. [30]. The loading noses translate vertically to induce a pure shear stress load distribution on the 10 × 10 mm coupons. All specimens were loaded with a 0.2 mm gap between the loading noses to ensure shearing of the midplane as ply thicknesses were 0.1 mm preconsolidation. Manually adjustable support blocks were used to ensure symmetrical and flush alignment to the loading noses without gaps. The CST device was placed in a universal testing machine (4505, Instron USA) with a 100kN load cell. Five specimens from each graphene loading condition were tested at a 1 mm/min displacement rate. Samples that failed due to a 30% load drop but did not shear were excluded from the data set in accordance with ASTM D2344 [31]. The shear strength (σ) was calculated as a function of maximum compressive force (F_{peak}), length (l) and width (w) of the specimen according to Eq. 2.

$$\sigma = \frac{F_{peak}}{l \times w} \tag{2}$$

Micro-computed tomography

X-ray micro-computed tomography (μCT) was utilised to characterise the microstructure and further investigate in 3D the quality of consolidated CF/PEEK Control and graphene specimens. This technique is increasingly used for

composite characterisation providing detailed insights of the material architecture [32, 33] and has recently proven successful to characterise in detail the microstructure and map and quantify void distribution and content in CF/PEEK samples of comparable volumes [34]. The samples were imaged using an HeliScan™ micro-CT instrument hosted at the ANU CTLab, equipped with a 60 kV X-ray micro-focus source and a 3040×3040 pixels flat panel detector. Individual specimens were placed on a rotating motor-controlled stage with radioscope projections taken after each interval of rotation. Total acquisition time was about 9 h for each sample. The acquired 2D projections were processed using a proprietary ANU reconstruction algorithm [35] to create grey-scale 16-bit 3D volumetric images of the composites geometry at a scanning resolution (i.e. voxel size) of 2.0 µm. Image processing and quantitative analysis (i.e. segmentation) of void contents, as well as detail 3D mapping of void distribution within the samples' microstructure, were carried out using Mango, the software for image enhancement, parallel segmentation and network generation developed at the ANU specifically to work with tomographic data [36]. For selected portions of the samples, micro-CT volumetric data was then rendered in 3D using Drishti [37].

Results and discussion

Thin film FTIR and Raman spectroscopy

The graphene thin film was studied to understand the effects heat treatment had on the properties and substrate. The substrates and thin films were weighted before and after heat treatment to understand if heat treatment resulted in mass loss. The mean weight reduction of the GTF (HT) was 60% (13 ± 0.8 mg) compared to the marginal 0.12% (681 ± 12.9 mg) weight reduction of the CF/PEEK substrate. The significant weight reduction in the GTF (HT) sample strongly suggests surfactant removal with heat treatment. The mass loss in the CF/PEEK substrate may be from either sizing or moisture. Fourier transform infrared (FTIR) was conducted to study the chemical differences before and after the heat treatment process of the CF/PEEK substrate and GTF samples. The spectral data shows no chemical changes from the heat treatment process other than a small peak reduction in the spectra at 3428^{-1} (H–O-H) and 3629 cm^{-1} (-OH) suggesting removal of excess water from the thin film and CF/PEEK substrate [38] (Fig. S1). Raman spectroscopy was conducted on the graphene thin films to ensure heat treatment didn't change the graphene quality. The characteristic graphene peaks shown in the Raman spectra (Fig. S2) remain unchanged with heat treatment, but fluorescence is shown to reduce in the GTF (HT) sample compared to the GTF sample suggesting the removal of surfactant.

Optical microscopy, WLI, SEM and contact angle measurements

The thin film roughness was quantified with WLI to investigate changes to the thin film with heat treatment. The GTF was measured to have an absolute roughness of 1.56 ± 0.35 µm and root mean squared (RMS) roughness of 1.99 ± 0.36 µm (Fig. 2a). After heat treatment the roughness increased to an absolute roughness of

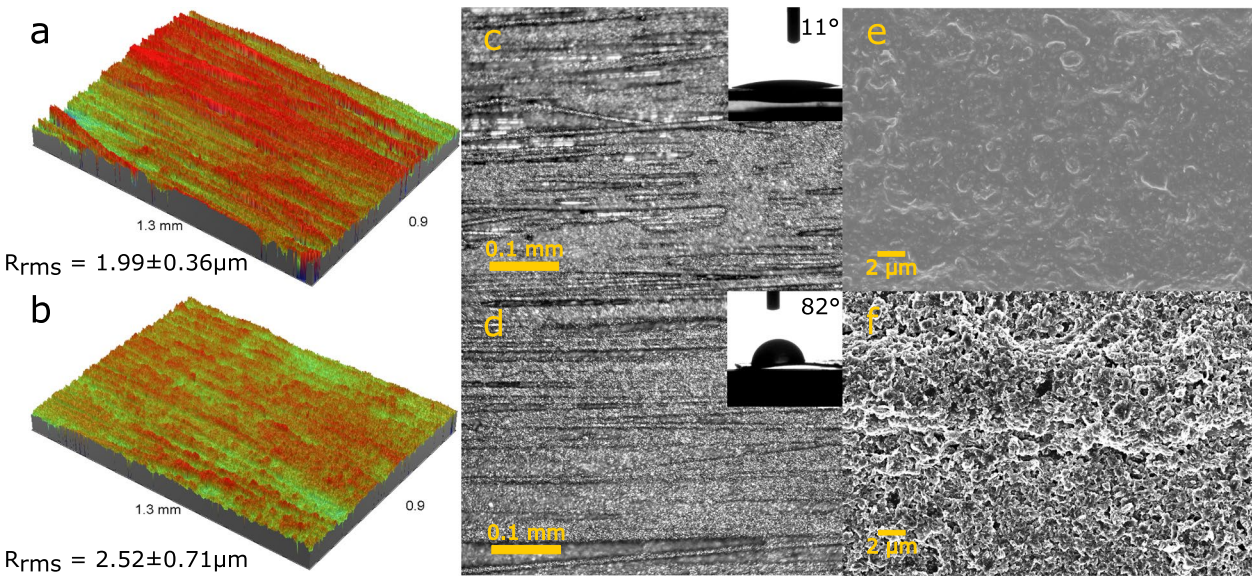

Fig. 2 **a** WLI surface map of GTF and (**b**) GTF (HT). **c** Optical image of GTF and (**d**) GTF (HT) sample with corresponding surface angle measurement inset. **e** SEM image of GTF and (**f**) GTF (HT)

1.99 ± 0.59 µm and an RMS roughness of 2.52 ± 0.71 µm (Fig. 2b). Optical images offer a qualitative visual of the thin film after spray deposition (Fig. 2c and d). Both GTF and GTF (HT) depict a visible uneven coating of the graphene thin film across the CF/PEEK substrate with fibres still visible through the thin film. Contact angle measurements of the graphene thin films were conducted with water to understand the wettability properties before and after heat treatment. The GTF demonstrated high wettability properties with a measured contact angle of approximately 11°. Comparatively, after heat treatment the wettability increases to 82°. The removal of surfactant during the heat treatment process is the likely cause of the substantial change in wettability of the graphene thin film [39].

The SEM image of the GTF (Fig. 2e) depicts smooth surface topology with poor graphene flake detail. Comparatively, the GTF (HT) image reveals detailed flakes upon a carbon fibre that are clearly visible (Fig. 2f). The difference in the SEM images of the graphene thin film is likely due to successful removal of excess surfactant. This visual difference in surface roughness correlates with the reduced surface wettability properties previously measured. Visual, chemical and qualitative measurements of the thin film before and after heat treatment validate successful removal of excess surfactant and excess water with little chemical effects to the graphene and CF/PEEK substrate quality.

Cross sectional Raman spectroscopy

The chemical quality of the graphene interlayer after consolidation was assessed using Raman spectroscopy (Fig. 3). The G and D peaks were fitted with a single Lorentzian curve at 1582 cm^{-1} and 1344 cm^{-1}, respectively, for both graphene enhanced samples. The G peak correlates with aromatic carbon stretching [40], while the D peak is activated when disorder and defects are present in the graphene [41, 42]. The D' peak located on the shoulder of the G peak at 1615 cm^{-1} helps determine additional information regarding the prominent type of defect present in the graphene sample [43]. The peak intensity ratio $I_D/I_{D'} = \sim 2.8$ and 2.5 for GL and GL (HT), respectively, corresponding to edge defects being the most common within the sample [12]. The lower peak intensity in GL (HT) is likely due to the heat treatment step reducing the grain boundaries present within the graphene flakes. Disorder in the form of topological defects, corrugations and atomic vacancies in the graphene sheets will also result in the D + D' seen at 2930 cm^{-1} [42, 43]. The I_D/I_G ratio is used to determine the disorder of the graphene and was approximately 0.8 for both GL and GL (HT). This corresponds disrupted sp^2 bonds and high graphite like structures likely due to the compact nature of consolidated thin films [44].

The 2D peak helps attain insights into the number of graphene layers after LPE and the heat treatment process [45]. The 2D peak for few layer graphene is typically fitted with 4 Lorentzian peaks corresponding to the electron interactions with the valance and conduction bands

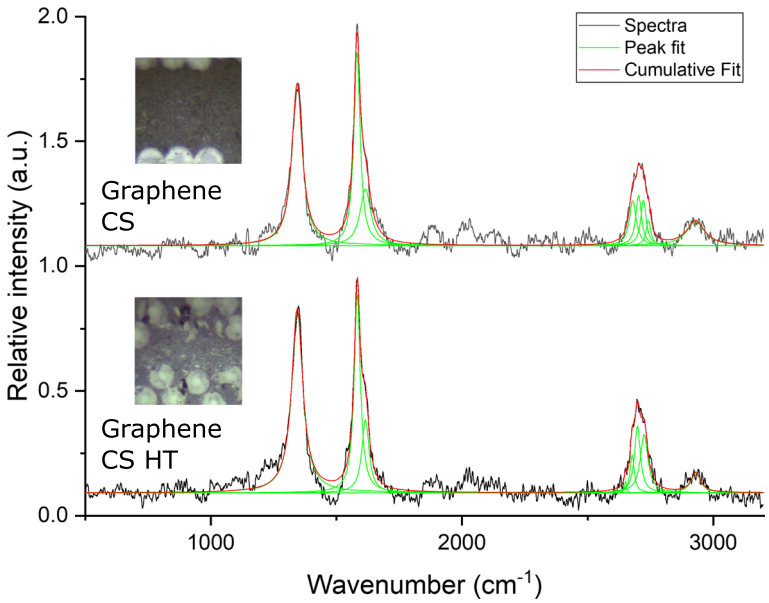

Fig. 3 Cross sectional (CS) Raman spectra of 1 wt% graphene additions, with and without heat treatment. Acquired spectra were obtained from the interlaminar region of the inset images

splitting into four phonons with opposite paired momentums [46]. The four bands appeared at 2667, 2686, 2708, 2732 cm^{-1} and 2650, 2677, 2698, 2725 cm^{-1} for GL and GL (HT), respectively. The I_D/I_{2D} ratio for GL and GL (HT) is 2.2 and 2.1, respectively, corresponding to ~ 5 layered graphene [47]. The full width half maximum (FWHM) of the 2D peak for GL is centred at 61 suggesting 3–4 layered graphene, while for GL (HT) at 57 corresponding to three layered graphene [48]. The fewer graphene layers suggest the graphene properties tend towards the theoretical intrinsic properties exhibited by monolayered graphene [49]. The conducted Raman analysis indicates that the spray-deposited graphene thin films with heat treatment are suited to functionalising carbon fibre composites.

Backscatter SEM and C-AFM

Backscatter SEM images of the graphene interlayer region are shown in Fig. 4. The graphene interlayer remains visible between the round carbon fibres after consolidation for both heat treated and non-heat treated samples. The GL sample has a more uneven graphene interlayer measuring approximately 9 µm in thickness (Fig. 4a). Comparatively, GL (HT) has a more uniform and compact graphene interlayer with a thickness of ~ 5 µm (Fig. 4b).

The C-AFM measurements were taken on cross-sectional graphene enhanced CF/PEEK samples to understand the effects of heat treatment on the nanoscale electrical conductivity characteristics within the interlayer region. Figure 4c depicts the electrically conductive nature of the 0° carbon fibres (yellow) on the nanoamp scale. Surrounding the fibres is the insulative PEEK matrix (black) which is expected due to the conductivity properties being many magnitudes less (10^{-18} S/cm [50]). The carbon fibres and graphene interlayer had optical density measurements of 49 and 81, respectively. This correlated to an average electrical

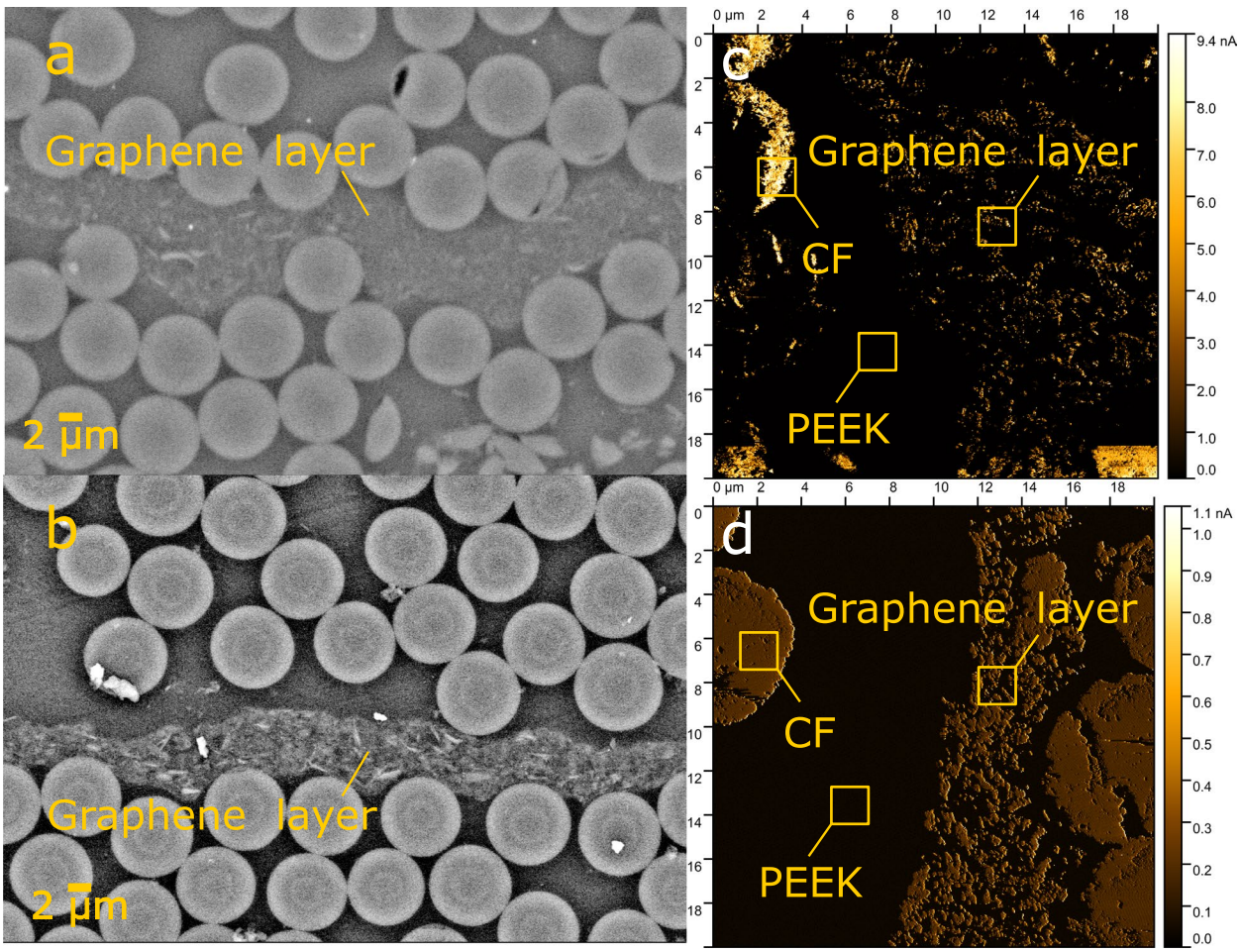

Fig. 4 **a** Backscatter SEM image of GL and (**b**) GL (HT) with the graphene interlayer region annotated. Annotated conductivity maps of (**c**) GL and (**d**) GL (HT) interlayer region

conductivity of 1.8 nA for the fibres and 3.0 nA for the graphene interlayer. The conductivity map of the GL (HT) sample is shown in Fig. 4d. The optical densities measured were 38 and 118 for carbon fibres and the graphene interlayer, respectively. The correlated electrical conductivities were 0.2 nA and 0.5 nA respectively.

The conductivity of GL (HT) measured approximately one magnitude lower than the GL sample. Tunnel current may be the mechanism resulting in the localised regions of high current observed in the interlaminar region of the GL sample [51]. The conductive networks were more concentrated and consistent in the interlayer region of the GL (HT) sample suggesting that a reduction in excess surfactant in the thin film translated to fewer insulative surfactant regions interfering with creating conductive networks. Successful use of graphene additions create physical connections or quantum tunnelling effects linking conductive domains (i.e. fibres and graphene) to bridge the insulative matrix region [52].

Greater consistency of the graphene thin films to create these conductive networks ensures uniform conductivity across the domain suitable for static change dissipation applications. These C-AFM measurements are 2D representations of 3D data as conductive networks can only be captured when current flows to the preamplifier due to the applied potential difference between the sample holder and the tip [53].

Interlaminar shear strength and void content

The void content was attained by digitally extracting and segmenting the voids in the reconstructed 3D tomogram images of the scanned samples. From this the compressive shear strength of the consolidated composites were plotted as a function of void content; shown in Fig. 5. The mean shear strength of CF/PEEK Control was measured to be 23.0 ± 3.5 MPa making it comparable to lap shear strength of hot gas torch automated tape placement (ATP) manufactured specimens [54]. After heat treatment of the Control, a 149% increase in shear strength was measured (57.2 ± 5.9 MPa). The Control (HT) sample performed 60% better than control samples fabricated using hot press methods in similar nanomaterial study [55]. The void content was substantially reduced with heat treatment from 4.2 vol% to 0.4 vol% for Control and Control (HT), respectively. The shear strength increased compared to the Control sample with the addition of 1 wt% graphene in the GL sample (31.39 ± 2.3 MPa), but the void content is the highest of all samples at 5.1 vol%. Comparably, the GL (HT) sample had a shear strength of 25.06 ± 3.4 MPa and a lower void content of 2.8 vol%. The substantial reduction in Control (HT) void content can be attributed to the removal of dissolved moisture absorbed during ambient storage of CF/PEEK prepreg tapes [56].

The shear strength of the composite is affected by the interfacial strength between the various material phases in the composite. Dispersion and van der Waals forces

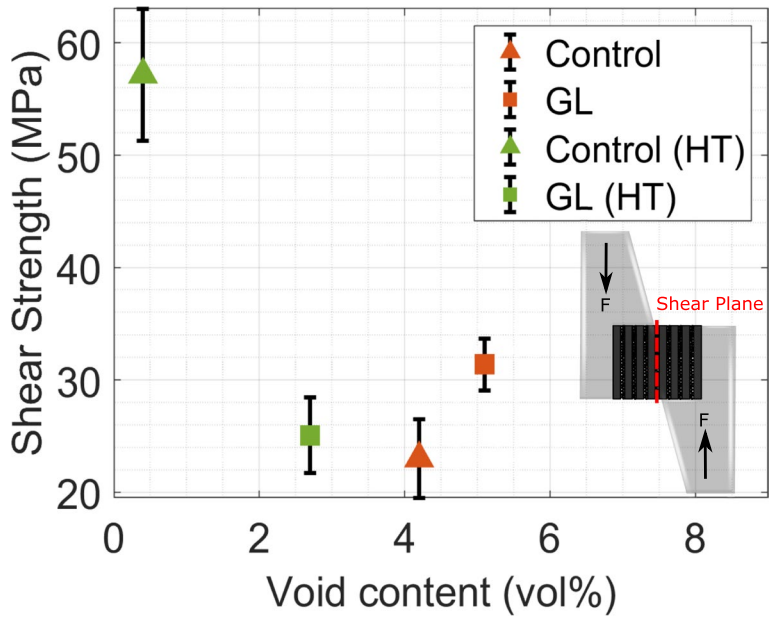

Fig. 5 Compressive shear strength of CF/PEEK Control samples and 1 wt% percent loading added to the interlaminar regions with and without heat treatment. All samples are within the range of an autoclave manufactured sample (25.70 ± 3.76 MPa) [54]. Error bars denote one standard deviation of the mean. The inset image depicts the interlaminar shear plane induced by the loading noses

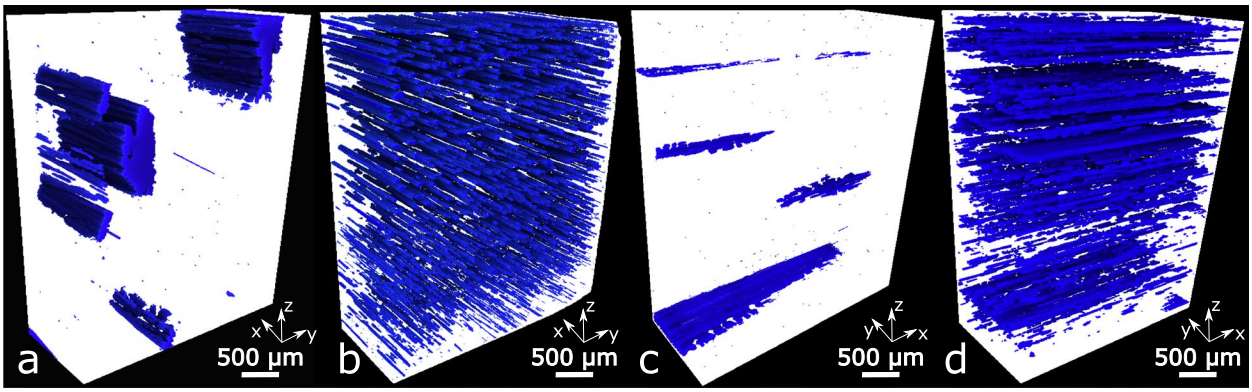

Fig. 6 3D void segmented image of (**a**) the Control (**b**) GL (**c**) Control (HT) and (**d**) GL (HT) samples. The images show voids in blue with matrix and fibres as 100% transparent

provide intermolecular bonding between the graphene and PEEK phases. The F68 surfactant adsorbs to the graphene during LPE, while the terminal –OH group in the surfactant chain may form a hydrogen bond with the oxygen-containing groups along the PEEK polymer chain, reinforcing the interface further. Additionally, increased surface roughness of the thin film after heat treatment aids mechanical interlocking between graphene and the PEEK matrix.

Similar studies with CNT additions to fibres [57] and graphene mixed homogeneously with the polymer matrix [58] had seen increased mechanical properties. Variations in sample thickness [23] and delamination effects [22] were found to reduce flexural and tensile strength properties of CF/epoxy composites with interlaminar nanomaterial additions. Studies utilising graphene oxide and functionalised PEEK to enhance mechanical properties result in an increase in scattering sites reducing overall conductive improvement [59].

The compressive shear strength induced in the interlaminar region suggests reduced bonding between plies due to a combination of voids and graphene additions. Limited matrix mixing with the graphene thin film will reduce the combined mechanical interlocking and chemical interactions resulting in the observed reduction in strength [55, 60]. Reductions in strength may also be a result of shearing within the thin film; whereby graphene sheets parallel to the shear plane provide little reinforcement. Voids concentrated within the interlaminar region will contribute to crack propagation and weaken interlocking between all phase interfaces weakening the mechanical strength of the composite [61]. Therefore, further investigation into the microstructure, and defect distribution was conducted by visualising µCT images.

Micro-computed tomography

Figure 6 depicts 3D visualisation of segmented images created on smaller yet representative volumes for the samples. The voids are shown in blue while the matrix and fibre phases are 100% transparent within the white volume. The segmented fibre and matrix phases were further used to calculate the fibre volume fraction (fvf). The Control sample (Fig. 6a) shows some large irregularly shaped voids permeating the length of the specimen with a fibre fraction of ~ 0.56. The segmented image of GL (Fig. 6b) clearly shows voids running parallel to the fibres permeating into the plies (fvf = ~ 0.59). The Control (HT) sample has the lowest number of voids in the volume compared to the other samples (Fig. 6c). The voids in Control (HT) also run parallel to the fibres but conform to the irregular shapes previously seen in the Control. The measured fvf of the sample was approximately 0.59, correlating with the information from the supplier. The GL (HT) sample has a more clustered distribution of voids concentrated within the interlaminar regions and not permeating into the plies (Fig. 6d). Concentration of voids within the interlaminar shear region correlate with the measured shear strength reduction in the GL (HT) sample. The structure of the voids continues to follow the same trend of long slender voids parallel to the plies independent of heat treatment. The measured fvf content is consistent with previous samples at ~ 0.59, suggesting consistent laminate consolidation using compression moulding.

Visual analysis of the 3D segmented images indicates that voids continue to form in the interlaminar region. This is likely due to the surfactant and moisture trapped in the thin film vapourising during high temperature processing [62-64]. The composite samples with heat treatment had reduced voids compared to their counterparts without heat treatment. The heat treatment step likely

contributed to the removal of excess surfactant and moisture in the thin film and substrate prior to consolidation. The reduced vapour sources have resulted in fewer voids forming and migrating into the intraply regions. The presence of voids in the GL (HT) sample suggests surfactant remains in the thin film even after processing in the oven.

Conclusions

This study investigated the effectiveness of heat treatment on graphene thin films and CF/PEEK substrates as a method to reduce voids in consolidated composites. Scalable manufacturing methods such as LPE and spray deposition were employed to create few layer graphene thin films on prepreg thermoplastic tapes. The removal of water was detected in the FTIR spectra after heat treatment but no additional chemical changes to the substrate and thin film were detected in the Raman and FTIR spectra. The graphene thin films became rougher with heat treatment increasing the RMS roughness from 1.99 µm to 2.52 µm. The heat treatment allowed for better visualisation of the graphene flakes while increasing surface wettability from 11° to 82°. The graphene quality was characterised to be 3–4 layers with Raman spectroscopy of the interlayer region after consolidation. The C-AFM measurements showed a higher concentration of conductive networks present in the interlaminar region after heat treatment.

The shear strength of the graphene enhanced laminate reduced 25% with heat treatment due to clustered voids within the interlaminar shear region. Heat treatment of the Control sample saw a 149% increase due to the removal of dissolved moisture within the PEEK thermoplastic. Although mechanical deficits were still measured, scalable graphene interlayer additions demonstrate incremental electrical improvements for insulative thermoplastic composite structures. Successful reduction in void content was achieved with heat treatment of the plies from 4.2 vol% to 0.4 vol%, and 5.1 vol% to 2.8 vol% in Control and graphene enhanced samples, respectively. While, vapourisation of surfactant is likely the cause of long cylindrical voids between fibres it remains important in the liquid phase exfoliation manufacturing process. Surfactant additions aid dispersion and prevent agglomeration both in suspension and in the polymer matrix phase; thus it cannot be entirely removed. Heat treatment of the spray deposited graphene thin film has proven to be an effective mechanism to reduce voids in consolidated thermoplastic composites.

Heat treatment reduces voids through removal of surfactant and moisture saleably without the need for suspension dialysis or use of vacuum ovens. Open air processing with automated tape placement (ATP) may allow the surfactant and water vapour to be more easily dissipated prior to consolidation. Further investigations into understanding the effects between graphene loading, conductive enhancement and void formation is required.

Supplementary Information

The online version contains supplementary material available at https://doi.org/10.1186/s42252-023-00044-0.

Additional file 1: Fig S1. FTIR spectra of Control, Control (HT), GTF and GTF (HT) samples. Annotation outline peaks characteristic to PEEK and water. **Fig S2.** Raman spectra of graphene thin film on CF/PEEK substrate with and without heattreatment. **Fig S3.** Mechanicaltest experimental curves. **Figure S3a.** A representative compressive extension vs load plot of the GL (HT) sample. **Figure S3b.** A representative compressive extension vs load plot of the Control (HT) sample.

Acknowledgements

The authors acknowledge the scientific and technical assistance, of the Australian Microscopy & Microanalysis Research Facility at the Centre of Advanced Microscopy, ANU; ANU X-ray Computed Tomography laboratory (CTLab); and the support of ANFF ACT Node *(ANFF @ ANU)* in carrying out this research. The authors also acknowledge *FlexeGRAPH* for supplying the graphene suspension and *J. Bradby* and *C. Nothoff* for providing the facilities for sample preparation and expertise for Raman spectroscopy and measurements. *D. Nisbet* and *E. Mohamed* for providing facilities and expertise for FTIR.

Authors' contributions

C. Leow: Conceptualization, Methodology, Investigation, Formal analysis, Writing – Original Draft, Validation, Visualization. P. Kreider: Writing – review &; editing, Validation, Visualisation, Investigation, Conceptualization, Supervision. S. Sommacal: Writing – review &; editing, Methodology, Formal analysis, Data Curation, Visualization. C. Nothoff: Writing – review &; editing, Methodology, C-AFM experiment. P. Kluth: Writing – review &; editing, Supervision, Funding acquisition. P. Compston: Writing – review &; editing, Conceptualization, Supervision, Project administration, Funding acquisition. The author(s) read and approved the final manuscript.

Funding

This project was conducted within the ARC Training Centre for Automated Manufacture of Advanced Composites (IC160100040), supported by the Commonwealth of Australia under the Australian Research Council's Industrial Transformation Research Program.

Availability of data and materials

Datasets can be accessed upon request.

Declarations

Competing interests

The authors declare no competing interests.

Received: 30 November 2022 Accepted: 28 May 2023
Published online: 06 June 2023

References

1. Z. Liu, L. Wang, X. Hou, J. Wu, Investigation on dielectrical and space charge characteristics of peek insulation used in aerospace high-voltage system. IEEJ Trans. Electr. Electron. Eng. **15**, 172 (2020)
2. A.M. Díez-Pascual, M. Naffakh, M.A. Gómez, C. Marco, G. Ellis, M.T. Martínez, A. Ansón, J.M. González-Domínguez, Y. Martínez-Rubi, B. Simard, Development and characterization of PEEK/carbon nanotube composites. Carbon N. Y. **47**, 3079 (2009)

3. R. Yadav, M. Tirumali, X. Wang, M. Naebe, B. Kandasubramanian, Polymer composite for antistatic application in aerospace. Def. Technol. **16**, 107 (2020)
4. C. Lee, X. Wei, J.W. Kysar, J. Hone, Measurement of the elastic properties and intrinsic strength of monolayer graphene. Science (80). **321**, 385 (2008)
5. Y. Zhu, S. Murali, W. Cai, X. Li, J.W. Suk, J.R. Potts, R.S. Ruoff, Graphene and graphene oxide: synthesis, properties, and applications. Adv. Mater. **22**, 3906 (2010)
6. J. Wu, J. Chen, Y. Zhao, W. Liu, W. Zhang, Effect of electrophoretic condition on the electromagnetic interference shielding performance of reduced graphene oxide-carbon fiber/epoxy resin composites. Compos. Part B Eng. **105**, 167 (2016)
7. K.A. Imran, K.N. Shivakumar, Graphene-modified carbon/epoxy nanocomposites: electrical, thermal and mechanical properties. J. Compos. Mater. **53**, 93 (2019)
8. J. Joseph, P.R. Munda, D.A. John, A.M. Sidpara, J. Paul, Graphene and CNT filled hybrid thermoplastic composites for enhanced EMI shielding effectiveness. Mater. Res. Express **6**, 085617 (2019)
9. R. Raccichini, A. Varzi, S. Passerini, B. Scrosati, The role of graphene for electrochemical energy storage. Nat. Mater. **14**, 271 (2015)
10. H. Tao, Y. Zhang, Y. Gao, Z. Sun, C. Yan, J. Texter, Scalable exfoliation and dispersion of two-dimensional materials-an update. Phys. Chem. Chem. Phys. **19**, 921 (2017)
11. D.C. Marcano, D.V. Kosynkin, J.M. Berlin, A. Sinitskii, Z. Sun, A. Slesarev, L.B. Alemany, W. Lu, J.M. Tour, Improved synthesis of graphene oxide. ACS Nano **4**, 4806 (2010)
12. R. Narayan, J. Lim, T. Jeon, D.J. Li, S.O. Kim, Perylene tetracarboxylate surfactant assisted liquid phase exfoliation of graphite into graphene nanosheets with facile re-dispersibility in aqueous/organic polar solvents. Carbon N. Y. **119**, 555 (2017)
13. S. Lin, C.-J. Shih, M.S. Strano, D. Blankschtein, Molecular insights into the surface morphology, layering structure, and aggregation kinetics of surfactant-stabilized graphene dispersions. J. Am. Chem. Soc. **133**, 12810 (2011)
14. V.M. Samoilov, E.A. Danilov, A.V. Nikolaeva, G.A. Yerpuleva, N.N. Trofimova, S.S. Abramchuk, K.V. Ponkratov, Formation of graphene aqueous suspensions using fluorinated surfactant-assisted ultrasonication of pristine graphite. Carbon N. Y. **84**, 38 (2015)
15. S.M. Notley, Highly concentrated aqueous suspensions of graphene through ultrasonic exfoliation with continuous surfactant addition. Langmuir **28**, 14110 (2012)
16. M. Lotya, P.J. King, U. Khan, S. De, J.N. Coleman, High-concentration, surfactant-stabilized graphene dispersions. ACS Nano **4**, 3155 (2010)
17. U. Khan, A. O'Neill, M. Lotya, S. De, J.N. Coleman, High-concentration solvent exfoliation of graphene. Small **6**, 864 (2010)
18 D. Ager, V. ArjunanVasantha, R. Crombez, J. Texter, Aqueous graphene dispersions-optical properties and stimuli-responsive phase transfer. ACS Nano **8**, 11191 (2014)
19. X.F. Wu, A. Rahman, Z. Zhou, D.D. Pelot, S. Sinha-Ray, B. Chen, S. Payne, A.L. Yarin, Electrospinning core-shell nanofibers for interfacial toughening and self-healing of carbon-fiber/epoxy composites. J. Appl. Polym. Sci. **129**, 1383 (2013)
20. Y. Li, H. Zhang, Y. Liu, H. Wang, Z. Huang, T. Peijs, E. Bilotti, Synergistic effects of spray-coated hybrid carbon nanoparticles for enhanced electrical and thermal surface conductivity of cfrp laminates. Compos. Part A Appl. Sci. Manuf. **105**, 9 (2018)
21. H. Zhang, Y. Liu, M. Kuwata, E. Bilotti, T. Peijs, Improved fracture toughness and integrated damage sensing capability by spray coated CNTs on carbon fibre prepreg. Compos. Part A Appl. Sci. Manuf. **70**, 102 (2015)
22. S.S.A. Kumar, M.N. Uddin, M.M. Rahman, R. Asmatulu, Introducing graphene thin films into carbon fiber composite structures for lightning strike protection. Polym. Compos. **40**, E517 (2019)
23. V. Kumar, S. Sharma, A. Pathak, B.P. Singh, S.R. Dhakate, T. Yokozeki, T. Okada, T. Ogasawara, Interleaved MWCNT buckypaper between CFRP laminates to improve through-thickness electrical conductivity and reducing lightning strike damage. Compos. Struct. **210**, 581 (2019)
24. C. Leow, P.B. Kreider, C. Notthoff, P. Kluth, A. Tricoli, P. Compston, A Graphene film interlayer for enhanced electrical conductivity in a carbon-Fibre/PEEK composite. Funct. Compos. Mater. **2**, 1 (2021)
25. N.D. Mansukhani, L.M. Guiney, P.J. Kim, Y. Zhao, D. Alducin, A. Ponce, E. Larios, M.J. Yacaman, M.C. Hersam, High-concentration aqueous dispersions of nanoscale 2D materials using nonionic Biocompatible Block Copolymers. Small **12**, 294 (2016)
26. F.N. Cogswell, F. Neil, *Platen Pressing of Carbon Fibre/PEEK Laminates Thermoplastic Aromatic Polymer Composites Materials* (Butterworth Heinemann, Oxford, 1992), p.249
27. V. Chabot, B. Kim, B. Sloper, C. Tzoganakis, A. Yu, High yield production and purification of few layer graphene by gum Arabic assisted physical sonication. Sci. Rep. **3**, 1378 (2013)
28. F. Menges, Spectragryph - software for optical spectroscopy (version 1.2.15 [Software]. (2020). https://www.effemm2.de/
29. M.M. Lucchese, F. Stavale, E.H.M. Ferreira, C. Vilani, M.V.O. Moutinho, R.B. Capaz, C.A. Achete, A. Jorio, Quantifying ion-induced defects and raman relaxation length in graphene. Carbon N. Y. **48**, 1592 (2010)
30. V. Zinnecker, C.M. Stokes-Griffin, A. Khudiakova, M. Wolfahrt, P. Compston, A comparative study for shear testing of thermoplastic-based composites and metal-composite hybrids. Compos. Part A Appl. Sci. Manuf. **137**, 105953 (2020)
31. ASTM International, ASTM D2344/D2344M: Standard Test Method for Short-Beam Strength of Polymer Matrix Composite Materials and Their Laminates, ASTM Stand. D2344 **3**, 136 (2003).
32. S.C. Garcea, Y. Wang, P.J. Withers, X-Ray computed tomography of polymer composites. Compos. Sci. Technol. **156**, 305 (2018)
33. M. Mehdikhani, I. Straumit, L. Gorbatikh, S.V. Lomov, Detailed characterization of voids in multidirectional carbon fiber/epoxy composite laminates using x-ray micro-computed tomography. Compos. Part A Appl. Sci. Manuf. **125**, 105532 (2019)
34. S. Sommacal, A. Matschinski, K. Drechsler, P. Compston, Characterisation of void and fiber distribution in 3D printed carbon-fiber/PEEK using x-ray computed tomography. Compos. Part A Appl. Sci. Manuf. **149**, 106487 (2021)
35. G. R. Myers, A. M. Kingston, S. J. Latham, B. Recur, T. Li, M. L. Turner, L. Beeching, and A. P. Sheppard, Rapidly Converging Multigrid Reconstruction of Cone-Beam Tomographic Data, In. Developments in X-Ray Tomography X, edited by S. R. Stock, B. Müller, and G. Wang, Vol. 9967 (2016), p. 99671M.
36. A. Sheppard, S. Latham, J. Middleton, A. Kingston, G. Myers, T. Varslot, A. Fogden, T. Sawkins, R. Cruikshank, M. Saadatfar, N. Francois, C. Arns, T. Senden, Techniques in helical scanning, dynamic imaging and image segmentation for improved quantitative analysis with X-Ray Micro-CT. Nucl. Instruments Methods Phys. Res. Sect. B Beam Interact. with Mater. Atoms. **324**, 49 (2014)
37. A. Limaye, Drishti: A Volume Exploration and Presentation Tool, in edited by S. R. Stock (2012), p. 85060X.
38. L. Seema, M. Datta, Organoclay pluronic F68 – montmorillonite, as a sustained release drug delivery vehicle for propranolol hydrochloride. Eur. Chem. Bull. **3**, 593 (2014)
39. S. Pinto, P. Alves, C.M. Matos, A.C. Santos, L.R. Rodrigues, J.A. Teixeira, M.H. Gil, Poly (Dimethyl Siloxane) surface modification by low pressure plasma to improve its characteristics towards biomedical applications. Colloids Surfaces B Biointerfaces **81**, 20 (2010)
40. M.B. Vázquez-Santos, E. Geissler, K. László, J.N. Rouzaud, A. Martínez-Alonso, J.M.D. Tascón, Comparative XRD, Raman, and TEM Study on Graphitization of PBO-Derived Carbon Fibers. J. Phys. Chem. C **116**, 257 (2012)
41. M. Acik, Y.J. Chabal, Nature of graphene edges: a review. Jpn. J. Appl. Phys. **50**, 070101 (2011)
42. I. Childres, L. A. Jauregui, W. Park, H. Caoa, and Y. P. Chena, Raman Spectroscopy of Graphene and Related Materials, New Dev. Phot. Mater. Res. **403**, 403–418 (2013).
43. G. Yang, L. Li, W.B. Lee, M.C. Ng, Structure of graphene and its disorders: a review. Sci. Technol. Adv. Mater. **19**, 613 (2018)
44. H. Lu, Y. Yao, W.M. Huang, D. Hui, Noncovalently functionalized carbon fiber by grafted self-assembled graphene oxide and the synergistic effect on polymeric shape memory nanocomposites. Compos. Part B Eng. **67**, 290 (2014)
45. A.C. Ferrari, Raman spectroscopy of graphene and graphite: disorder, electron-phonon coupling, doping and nonadiabatic effects. Solid State Commun. **143**, 47 (2007)

46. A.C. Ferrari, J.C. Meyer, V. Scardaci, C. Casiraghi, M. Lazzeri, F. Mauri, S. Piscanec, D. Jiang, K.S. Novoselov, S. Roth, A.K. Geim, Raman spectrum of graphene and graphene layers. Phys. Rev. Lett. **97**, 1 (2006)
47. S. Gayathri, P. Jayabal, M. Kottaisamy, V. Ramakrishnan, Synthesis of few layer graphene by direct exfoliation of graphite and a raman spectroscopic study. AIP Adv. **4**, 027116 (2014)
48. Y. Hao, Y. Wang, L. Wang, Z. Ni, Z. Wang, R. Wang, C.K. Koo, Z. Shen, J.T.L. Thong, Probing layer number and stacking order of few-layer graphene by raman spectroscopy. Small **6**, 195 (2010)
49. A.C. Ferrari, D.M. Basko, Raman spectroscopy as a versatile tool for studying the properties of graphene. Nat. Nanotechnol. **8**, 235 (2013)
50. J.A. King, J.M. Tomasi, D.R. Klimek-McDonald, I. Miskioglu, G.M. Odegard, T.R. King, J.W. Sutherland, Effects of carbon fillers on the conductivity and tensile properties of polyetheretherketone composites. Polym. Compos. **39**, E807 (2018)
51. A. Summerfield, A. Kozikov, T.S. Cheng, A. Davies, Y.-J. Cho, A.N. Khlobystov, C.J. Mellor, C.T. Foxon, K. Watanabe, T. Taniguchi, L. Eaves, K.S. Novoselov, S.V. Novikov, P.H. Beton, Moiré-modulated conductance of hexagonal boron nitride tunnel barriers. Nano Lett. **18**, 4241 (2018)
52 R. Taherian, Experimental and analytical model for the electrical conductivity of polymer-based nanocomposites. Compos. Sci. Technol. **123**, 17–31 (2016)
53. G. Benstetter, A. Hofer, D. Liu, W. Frammelsberger, M. Lanza, *Fundamentals of CAFM Operation Modes, in Conductive Atomic Force Microscopy* (Wiley-VCH Verlag GmbH & Co. KGaA, Weinheim, Germany, 2017), pp.45–77
54. Z. Qureshi, T. Swait, R. Scaife, H.M. El-Dessouky, In situ consolidation of thermoplastic prepreg tape using automated tape placement technology: potential and possibilities. Compos. Part B Eng. **66**, 255 (2014)
55. H. Xu, X. Tong, Y. Zhang, Q. Li, W. Lu, Mechanical and electrical properties of laminated composites containing continuous carbon nanotube film interleaves. Compos. Sci. Technol. **127**, 113 (2016)
56. T.K. Slange, L.L. Warnet, W.J.B. Grouve, R. Akkerman, Deconsolidation of C/PEEK blanks: on the role of prepreg, blank manufacturing method and conditioning. Compos. Part A Appl. Sci. Manuf. **113**, 189 (2018)
57. E.A.M. Hassan, D. Ge, S. Zhu, L. Yang, J. Zhou, M. Yu, Enhancing CF/PEEK composites by CF decoration with polyimide and loosely-packed CNT arrays. Compos. Part A Appl. Sci. Manuf. **127**, 105613 (2019)
58. L. Liu, L. Xiao, X. Zhang, M. Li, Y. Chang, L. Shang, Y. Ao, Improvement of the thermal conductivity and friction performance of poly (Ether Ether Ketone)/carbon fiber laminates by addition of graphene. RSC Adv. **5**, 57853 (2015)
59. Y. Hwang, M. Kim, J. Kim, Improvement of the mechanical properties and thermal conductivity of poly (Ether-Ether-Ketone) with the Addition of Graphene Oxide-Carbon Nanotube Hybrid Fillers. Compos. Part A Appl. Sci. Manuf. **55**, 195 (2013)
60. P.Y. Hung, K.T. Lau, B. Fox, N. Hameed, J.H. Lee, D. Hui, Surface modification of carbon fibre using graphene-related materials for multifunctional composites. Compos. Part B Eng. **133**, 240 (2018)
61. X. Gao, Z. Huang, H. Zhou, D. Li, Y. Li, Y. Wang, Higher Mechanical Performances of CF /PEEK Composite Laminates via Reducing Interlayer Porosity Based on the Affinity of Functional S-PEEK. Polym. Compos. **40**, 3749 (2019)
62. A. Mirabedini, A. Ang, M. Nikzad, B. Fox, K.T. Lau, N. Hameed, Evolving strategies for producing multiscale graphene-enhanced fiber-reinforced polymer composites for smart structural applications. Adv. Sci. **7**, 1903501 (2020)
63. F. Hussain, M. Hojjati, M. Okamoto, R.E. Gorga, Review article: polymer-matrix nanocomposites, processing, manufacturing, and application: an overview. J. Compos. Mater. **40**, 1511 (2006)
64. A.R. Chambers, J.S. Earl, C.A. Squires, M.A. Suhot, The effect of voids on the flexural fatigue performance of unidirectional carbon fibre composites developed for wind turbine applications. Int. J. Fatigue **28**, 1389 (2006)

Publisher's Note